EFDA–JET–CP(14)01/43

M.I. Airila, A. Järvinen, M. Groth, P. Belo, S. Wiesen, S. Brezinsek,
K. Lawson, D. Borodin, A. Kirschner, J.P. Coad, K. Heinola,
J. Likonen, M. Rubel, A. Widdowson and JET EFDA contributors

Beryllium Migration During JET ITER-LikeWall Divertor Operation

Beryllium Migration During JET ITER-LikeWall Divertor Operation

M.I. Airila[1], A. Järvinen[2], M. Groth[2], P. Belo[3], S. Wiesen[4], S. Brezinsek[4], K. Lawson[5], D. Borodin[4], A. Kirschner[4], J.P. Coad[1], K. Heinola[5,6], J. Likonen[1], M. Rubel[7], A. Widdowson[5] and JET EFDA contributors*

JET-EFDA, Culham Science Centre, OX14 3DB, Abingdon, UK

[1]VTT Technical Research Centre of Finland, PO Box 1000, 02044 VTT, Finland
[2]Department of Applied Physics, Aalto University, PO Box 14100, 00076 AALTO, Finland
[3]Instituto de Plasmas e Fusão Nuclear, Instituto Superior Técnico, Av Rovisco Pais, 1049-001 Lisbon, Portugal
[4]Forschungszentrum Jülich, Institut für Energie- und Klimaforschung Plasmaphysik, 52425 Jülich, Germany
[5]Culham Centre for Fusion Energy, Abingdon OX14 3DB, UK
[6]University of Helsinki, PO Box 43, 00014 University of Helsinki, Finland
[7]Royal Institute of Technology, Fusion Plasma Physics, 10044 Stockholm, Sweden
** See annex of F. Romanelli et al, "Overview of JET Results", (24th IAEA Fusion Energy Conference, San Diego, USA (2012)).*

Preprint of Paper to be submitted for publication in Proceedings of the
21st International Conference on Plasma Surface Interactions, Kanazawa, Japan
26th May 2014 – 30th May 2014

ABSTRACT
Migration of beryllium into the divertor and deposition on tungsten in the final phase of the first ITER-like-wall campaign of JET are modelled with the 3D Monte Carlo impurity transport code ERO. The simulation covers the inner wall and the inner divertor. To generate the plasma background for Monte Carlo tracing of impurity particles, we use the EDGE2D/EIRENE code set. At the wall, the estimated plasma conditions are $T_e \approx 5$eV and $n_e \approx 2 \times 10^{17}\mathrm{m}^{-3}$ (far-scrape-off layer; more than 10cm away from the LCFS). Relevant sputtering yields of beryllium (atomic and BeD) were determined in [1]. We calculate impurity distributions in the plasma using the main chamber source as a free parameter in modelling and attempt to reproduce inter-ELM spectroscopic Be II line (527nm) profiles at the divertor. The present model does not give satisfactory agreement, but further work will focus on fulfilling this constraint and ultimately link the modelled poloidal net deposition profiles of beryllium to post mortem data.

1. INTRODUCTION
The ITER first-wall material mix of beryllium and tungsten is being tested at JET to gain understanding on the durability and plasma compatibility of such a metallic environment. The main motivation of discarding carbon completely in plasma-facing components is its tendency to accumulate tritium in co-deposits. Indeed, already the first ITER-like wall (ILW) campaign soon confirmed a large reduction in impurity release and hydrogen retention rate compared to an all-carbon machine [2, 3]. However, further analysis is required for other major differences between JET-C and JET-ILW, related to wall durability and plasma operation in eventually high-performance scenarios. This contribution focuses on changes in wall composition due to material mixing, specifically beryllium migration from the main wall to the tungsten divertor.

After the installation of the ILW, it was anticipated that eroded beryllium from the main wall is transported to the tungsten divertor and form mixed-materials. Indeed, significant changes in the divertor composition were already evident from the evolution of spectroscopic signals and related modelling in the very first phase of the campaign [4]. For a detailed investigation of the resulting deposits and possible mixed materials, the first experimental year with the ILW was concluded with a long series of identical H-mode discharges, followed by removal and detailed analysis of selected samples from the first wall [5–8]. The surface analysis methods include IBA, SIMS and tile profiling at the divertor. Spectroscopic observations of the Be I line (457nm) indicate that steady conditions at the divertor were achieved rapidly (about in 1 day) in this experiment, as illustrated in Figure 1. Such conditions are favourable for modelling, although the plasma-facing components carry the complete history over the campaign, which must be eventually taken into account by simulating divertor surface evolution starting from a range of different initial states. In this work we only present simulations that assume initially clean tungsten surface.

We simulate the migration of beryllium eroded from the main wall into the divertor and deposition on tungsten in the final operation phase with the 3D Monte Carlo impurity transport code ERO [9].

The simulation covers the inner wall and the inner divertor as shown in Figure 2. To generate the plasma background for MC tracing of impurity particles, we use the EDGE2D/EIRENE code set [10–12]. At the wall, the estimated plasma conditions are $T_e \approx 5$eV and $n_e \approx 2 \times 10^{17}\text{m}^{-3}$ (far-scrape-off layer; more than 10 cm away from the LCFS). In addition to the SOL plasma, charge-exchange neutrals are believed to contribute significantly to the main wall erosion. Relevant sputtering yields of beryllium (atomic and BeD) were determined in [1]. We compare the modelled impurity densities in the plasma and their temporal evolution to the spectroscopic Be II line (527 nm) profiles at the divertor. With this constraint, we link the modelled poloidal net deposition profiles of beryllium to post mortem data.

2. EXPERIMENT

The JET campaign C30c in July 2012 consisted of 151 successful H-mode discharges in deuterium (906s flattop / 2500s divertor plasma time in total) with the inner strike point on Tile 3, the outer strike point on the horizontal Tile 5, I_p = 2.0MA, B_t = 2.0T, and P_{aux} = 11.5MW (NBI). The ELM frequency was between 25–40Hz, ELM size being about 100kJ calculated from the MHD and diamagnetic energy variation of the plasma.

Be II emission in the divertor was comprehensively diagnosed using the vertical, poloidally scanning VUV and visible spectrometer (KT1) and a fast visible spectrometer with 10 channels looking both at the inner and outer divertor (KS3/EDG8). Both signals can be filtered for ELMs, giving mutually consistent interand intra-ELM profiles when the signal from the scanning spectrometer is corrected for the known loss of sensitivity (from a comparison to the D_α, D_β, Be II and C III lines at the visible horizontal view to NB shine-through areas, KS8). Also reconstructions from narrowband filtered CCD cameras for divertor imaging spectroscopy are well in line with the spectrometers. For lower intensities the background is believed to be significant compared to the Be II signal. Also BeD emission is seen in the scrape-off layer on Tile 1.

Post mortem analysis of a certain set of ILW tiles was planned already before installing them in the vessel. These tiles received marker coatings containing suitable interlayers that help in determining erosion and deposition after exposure, and were pre-characterized to provide an optimal basis for post mortem analysis. After about one year of operation, the selected tiles, including divertor tiles 1, 3, 4, 6, 7 and 8, a high-field gap closure tile (HFGC) inboard of the top of the inner divertor, and two tiles outboard of the outer divertor, were removed from the vessel. They were analysed using several techniques, including ion beam analysis (IBA) and tile profiling. For the present work the following observations from post mortem analysis of the inner divertor tiles are essential:

- Thick Be layer – about 10μm – on the horizontal surface of Tile 1 (inner divertor apron) and also on the plasma-exposed areas of the HFGC tile [8].
- Decreasing Be deposition towards the divertor base [5].

It would be possible to interpret the complete process of material migration if sufficiently accurate data were available both on erosion, plasma transport and deposition. For the present experiment the last two pieces of data (spectroscopic observations and post mortem analyses) are very satisfactorily fulfilled. However, as far as the beryllium source is concerned, there are at least two significant contributions: (i) erosion of the inner wall guard limiters both in limiter and divertor phases, and (ii) energetic charge-exchange neutrals that impact the whole wall especially in the divertor phase. In particular, the beryllium eroded in the limiter phase enters easily the core, is confined there and continues to diffuse out during the divertor phase [5, 13–15]. We start with a simple approach to verify the main characteristics of the migration, neglecting the details of erosion and penetration of beryllium, and focus only on the second step of the analysis: explaining the link between observed emission and deposition measurements. Modelling of the main chamber erosion is carried out separately [15] and those results may provide valuable input for an extended analysis of the complete migration chain in the future.

3. FLUID AND MONTE CARLO IMPURITY MODELLING

The multi-fluid code package EDGE2D/EIRENE was used to generate steady-state, interELM background plasma solutions for particle tracing with the ERO code. The cross-field transport coefficients for heat conduction and particle diffusion were adjusted to reproduce the experimental electron density and temperature profiles at the outer mid-plane measured with the high resolution Thomson scattering system (HRTS [16]). Calculated 2D plasma profiles were extrapolated exponentially to bridge the gap between the grid edge and vessel wall. As shown in Figure 3, three outer mid-plane densities were considered to span through the uncertainty of the high field side divertor conditions measured with Langmuir Probes (LP [17]). The LP data were filtered for ELMs and represent the phase between 70–95% of the inter-ELM period.

The present ERO model traces full orbits of test impurity particles in a rectangular simulation volume taking into account electromagnetic forces, frictional flow, ionization and reflection. Particles can originate either from an external source or physical sputtering. Chemical erosion is neglected for the time being because of its strong dependence on the substrate temperature. It is known that the sputtering in the form of BeD molecules can increase the total yield by 50% above the physical sputtering yield [1], and this can be taken into account if surface temperature data is available.

For technical reasons the 3D ERO model is currently limited to a toroidally symmetric wall geometry and plasma background. Therefore we cannot directly use a beryllium source consisting of separate components representing realistically the limiter and recessed area erosion. Instead, the source was approximated by an artificial distribution that would reproduce the observed emission. In this work we used atomic point sources of varying location and intensity near the inner midplane but did not yet achieve a satisfactory match to emission. As a test case we also defined an artificially high beryllium content of 4% in the plasma instead of the point source. Figure 4 (base case plasma background) shows that the simulated level of emission is correct close to the inner wall in both of these cases, but decreases rapidly outwards, while the measured emission peaks at $R \approx 2.4$m in the actual divertor region. One explanation for this discrepancy is particle leakage from the ERO simulation, but was diagnosed to constitute only about 15% of the source rate and cannot therefore be the only reason. It is more likely that migration through the outer scrape-off layer, which is missing from the simulation, brings in a significant contribution to beryllium emission in the divertor. It is also worth noting that the spectroscopic sightlines traverse the whole plasma chamber, thus collecting photons from a significantly longer distance than the synthetic diagnostic sampling only the simulation volume of ERO. The low-density case did not differ much from the base case, and in the high-density case the emission was even more localized.

Emission clouds and corresponding impurity density distributions are shown in Figure 5. Most of the beryllium is ionized to charge states > 1 in the divertor. This seems to limit the level of Be I and Be II emission in the simulations and hints that EDGE2D/EIRENE may overestimate the plasma background temperature in this region.

It is interesting to note that the erosion/deposition profiles are rather robust across different simulation cases, and qualitatively similar net deposition profile as observed in post mortem analysis (see Figure 6):

- Significant deposition on the HFCG tile (x_{ERO} = 720–800mm)
- Peak value on top of Tile 1 ($x_{ERO} \approx$ 820mm)
- Weak deposition elsewhere in the divertor.

Even the quantitative correspondence of the profiles is rather good. While the amount of deposited beryllium on the inner divertor has been estimated in [5] to 25.8cm^3 (average of 6.6×10^{19}at/s over the 47000s of plasma time), the present simulations were run with a higher estimated source rate and the results normalized afterwards. Due to nonlinearities in the surface behaviour the modelled net deposition should be corrected upwards. On the other hand, several factors contributing to re-erosion are still missing from the model and discussed below.

4. RESULTS AND DISCUSSION

We have analysed the the period of 151 identical H-mode plasma discharges (JET Pulse No: 83621–83795), which aimed at achieving well-defined wall conditions prior to the removal of longterm surface samples for post mortem analysis. While the complete material migration chain from erosion source to final deposition is yet too complex to model, our spectroscopic analysis of Be II emission and detailed post mortem data provide a solid basis to link the plasma impurity content to observed beryllium deposition on the tungsten divertor. Our present model matches the emitted Be II intensity close to the inner wall but not deeper in the plasma. In any case, the modelled deposition profiles are rather robust with respect to model variations and show the essential features present in the post mortem data. Even if the simulated beryllium source rate is adjusted to the amount of beryllium found on the inner divertor, the net deposition rate is slightly overestimated, but on the other hand, significant mechanisms contributing to re-erosion are still missing from our migration model. It is possible to gain much further insight to ILW-specific material migration issues by improving the computational model as follows:

- As a new, more flexible geometry model of ERO [18] is available soon, the simulation volume can be increased to encompass both divertor legs simultaneously, which avoids artificial leakage of impurities out of the simulation.
- Obviously the beryllium influx falls in the range where a homogeneous material mixing model predicts net deposition but in reality the enhanced sputtering by the presence of heavy tungsten atoms is sufficiently strong and prevents layers from building up. This phenomenon could be captured by using more complex, coupled ERO-SDTrimSP simulations [19] in which the ion-solid interaction model is based on the binary collision approximation.
- Our model is presently lacking the erosion due to ELMs. Recent time-dependent modelling of the ELM cycle with EDGE2D/EIRENE potentially allows inclusion of their effect in the model [20]. It may be necessary to run much longer ERO simulations with decreased spatial accuracy to capture the temporal evolution in the presence of ELMs.
- Chemical erosion of beryllium (BeD molecule release) is strongly dependent on the substrate temperature, varying from negligible to up to 50% of the physical sputtering yield at temperatures relevant to JET [1].

ACKNOWLEDGEMENTS
This work was supported by EURATOM and carried out within the framework of the European Fusion Development Agreement. The views and opinions expressed herein do not necessarily reflect those of the European Commission.

REFERENCES

[1]. S. Brezinsek et al., Europhys. Conf. Abs. **37D** (2013) P2.021.
[2]. J.W. Coenen et al., Nuclear Fusion **53** (2013) 073043.
[3]. S. Brezinsek et al., Nuclear Fusion **53** (2013) 083023.
[4]. K. Krieger et al., Journal of Nuclear Materials **438** (2013) S262.
[5]. A. Widdowson et al., Physica Scripta **T159** (2014) 014010.
[6]. J.P. Coad et al., Physica Scripta **T159** (2014) 014012.
[7]. K. Heinola et al., Physica Scripta **T159** (2014) 014013.
[8]. K. Heinola et al.., these proceedings.
[9]. A. Kirschner et al., Nuclear Fusion **40** (2000) 989.
[10]. R. Simonini et al., Contributions to Plasma Physics **34** (1994) 368.
[11]. D. Reiter, Journal of Nuclear Materials **196–198** (1992) 80.
[12]. S. Wiesen, EDGE2D/EIRENE code interface report, JET ITC-Report, http://www.eirene.de/e2deir report 30jun06.pdf, 2006

[13]. J. Miettunen et al., Journal of Nuclear Materials **438** (2013) S612.
[14]. D. Borodin et al., Journal of Nuclear Materials **438** (2013) S267.
[15]. D. Borodin et al., Physica Scripta **T159** (2014) 014057.
[16]. M.N.A. Beurskens et al., Nuclear Fusion **48** (2008) 095004.
[17]. R.D. Monk et al., Journal of Nuclear Materials **241–243** (1997) 396.
[18]. D. Matveev et al., these proceedings.
[19]. S. Droste et al., Plasma Physics and Controlled Fusion **50** (2008) 015006.
[20]. D. Harting et al., these proceedings.

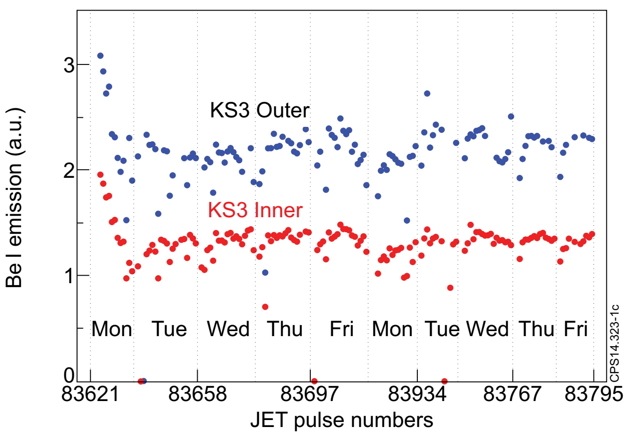

Figure 1: Evolution of Be I emission intensity in outer (blue) and inner (red) divertor during the campaign C30c. Practically steady-state conditions were achieved during the first day.

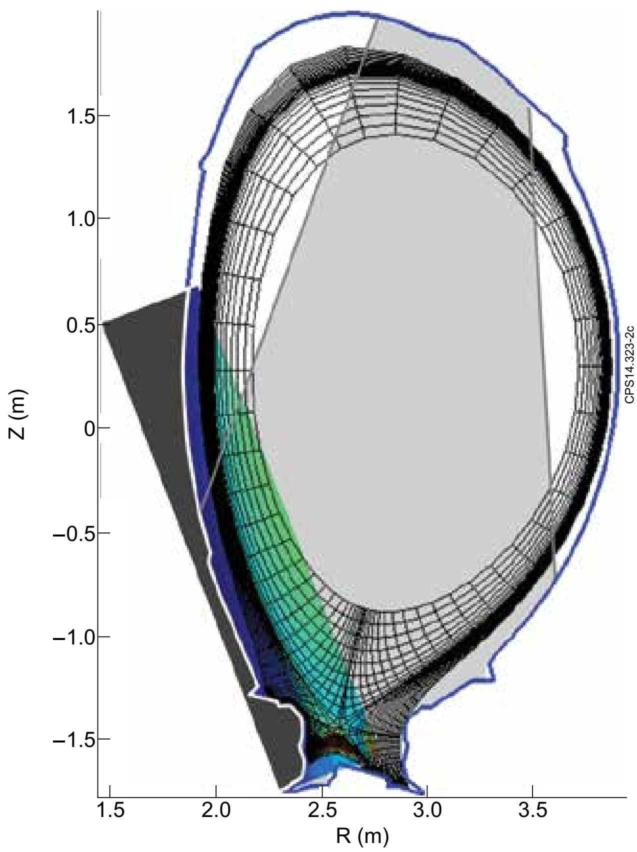

Figure 2: Modelling geometry for EDGE2D/EIRENE (black mesh) and ERO (rectangular volume showing the inter-ELM plasma density colormap) as well as the view of the vertical poloidally scanning visible spectrometer.

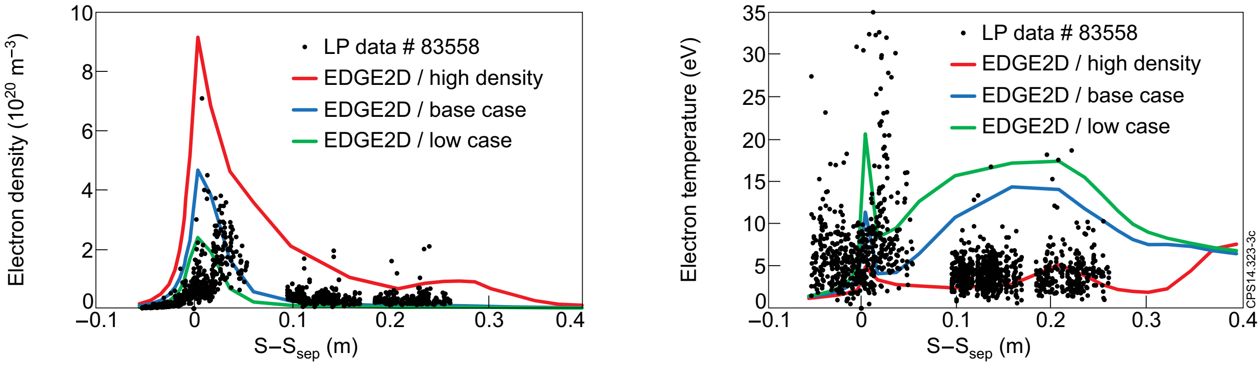

Figure 3: Plasma parameters calculated with EDGE2D/EIRENE at the inner divertor target and corresponding Langmuir probe measurements acquired during a strike-point sweep. The probe data were filtered to represent only the period 70–95% of inter-ELM phases.

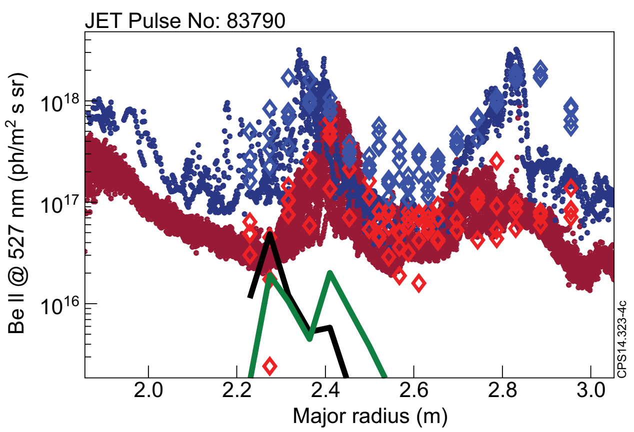

Figure 4: Comparison of modelled Be II emission to the poloidally scanning visible spectrometer (dark blue dots: intra-ELM, dark red dots: inter-ELM; corrected for loss of sensitivity) and visible high-time-resolution spectrometer (blue diamonds: intra-ELM, red diamonds: inter-ELM). The simulation cases shown represent point source assumption (black line) and 4% background beryllium assumption (green line) after 60s of simulation. In the last case only emission from re-eroded deposits is accounted for.

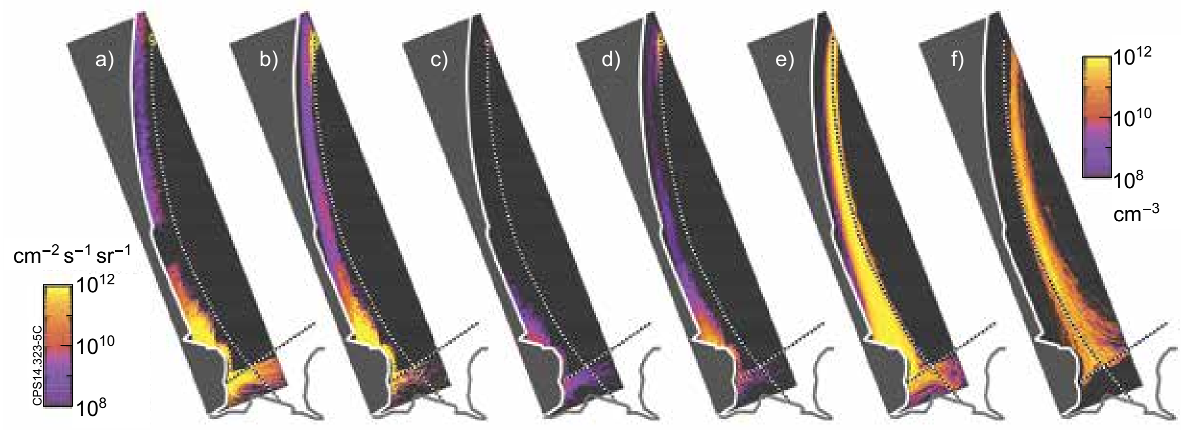

Figure 5: Modelled 2D emission and density disributions for beryllium. (a) Be I emission, (b) Be II emission, (c) Be^0 neutral density, (d) Be^+ ion density, (e) Be^{2+} ion density and (f) Be^{4+} ion density. The artificial Be^0 source is seen as a bright spot at the top, and physically eroded Be^0 shows up at the walls. The higher the temperature (further from the wall), the higher charge state dominates the distribution.

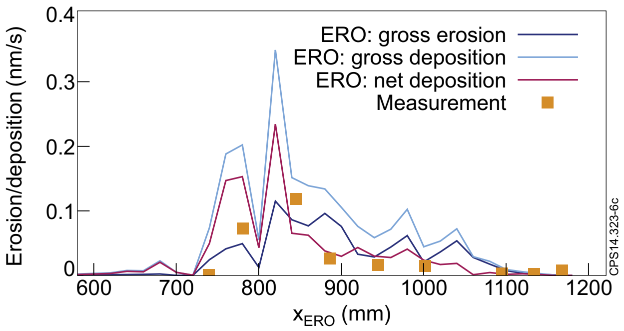

Figure 6: Modelled steady-state erosion/deposition balance compared to the measured deposition profile. The simulation results were scaled to correspond to the estimated source rate $25.8cm^3/47000s = 6.6 \times 10^{18}$ atoms/s from the inner wall of the main chamber.